# Bifurcation Analysis of Higher *m*:*n* Resonance Spectroscopic Hamiltonian†

**John F. Svitak, Vivian Tyng, and Michael E. Kellman***

*Department of Chemistry, University of Oregon, Eugene, Oregon 97403-1253*

*Received: June 27, 2002*

The classical phase space structure of a spectroscopic Hamiltonian for two coupled vibrational modes is analyzed using bifurcation theory, classified on catastrophe maps, for a variety of higher order resonances (3:2, 4:2, 5:2, 6:2 and 4:4, 5:4, 6:4), cases not considered in previous work. A type of bifurcation not encountered for lower resonance orders, based on *overlap of separatrices* rather than change in behavior of fixed points, is analyzed, and a procedure is developed to augment the catastrophe map. Energy level patterns are associated with the new resonances, in analogy with the patterns of adjacent level spacings considered earlier for the 2:1 resonance.

## I. Introduction

The fitting and interpretation of molecular vibrational spectra often requires resonance coupling terms in the spectroscopic Hamiltonian, in addition to terms diagonal in the number of quanta in the zero-order normal modes. These coupling terms mix the zero-order modes so that the eigenstates are no longer assignable, at least in a dynamically meaningful way, in terms of quantum numbers of the zero-order modes. Instead, new assignments of the number of quanta in modes that reflect the resonant dynamics are more properly used. Systems where this has been accomplished include local stretch modes,[1,2] resulting from a 2:2 Darling−Dennison resonance, and stretch−bend resonant modes,[3] resulting from a 2:1 Fermi resonance. This is done using tools of nonlinear dynamics including bifurcation and catastrophe map analysis.[4−6] Observable patterns in the spectra that reflect the changes in the dynamics have been predicted,[7] and these patterns have been exploited in analysis of spectra of isomerizing systems,[8] highly excited spectra of $CS_2$,[9] and spectra of chaotic bending dynamics of acetylene.[10,11]

In this paper, our previous analyses of the 2:2 and 2:1 resonance systems is generalized to higher-order resonance Hamiltonians with $m{:}n = m{:}2$ and $m{:}4$. There are several reasons for doing this. These resonances may arise by accident in arbitrary molecular spectra. They are known to be very relevant to the system of two coupled Morse oscillators, a frequently used model for a pair of coupled stretch vibrations.[12−18] As the coupling is varied between zero and infinity, the system tunes through a series of strong resonances of these types.[15−18] The coupled Morse oscillator model is directly relevant to the dynamics of the stretching normal modes of $CO_2$ and $CS_2$, where the frequency ratios of the modes imply a 4:2 resonance in $CO_2$ and a 5:2 resonance in $CS_2$.

We begin by introducing the spectroscopic fitting Hamiltonian and converting it to a corresponding semiclassical form in action-angle variables. Then, we discuss the fundamental modes of the classical system, that is, the low-energy normal modes and the new modes, born in bifurcations, that define the large-scale phase space structure. We use the catastrophe map to classify all types of dynamics possible for a spectroscopic Hamiltonian of given resonance order. Examination of the 3:2 resonance shows that this treatment is not quite complete: an additional bifurcation is found that does not directly involve the behavior of the fundamental modes, but rather *overlapping of separatrices*. A procedure is given to augment the catastrophe map to include this new bifurcation. Explicit catastrophe maps are presented for the 3:2, 4:2, 5:2, 6:2 and 4:4, 5:4, and 6:4 resonances, with discussion of spectral patterns associated with these systems.

## II. Semiclassical Resonance Hamiltonian

A spectroscopic fitting Hamiltonian to second order in the quantum numbers with a single *m*: *n* resonance coupling is given by

$$H_{m:n} = H_0 + V_{m:n} \tag{1}$$

where $H_0$ is the diagonal term up to second order in the normal modes

$$H_0 = \sum_i \omega_i \left(n_i + \frac{d_i}{2}\right) + \sum_i \sum_{j \geq i} \chi_{ij} \left(n_i + \frac{d_i}{2}\right)\left(n_j + \frac{d_j}{2}\right); \tag{2}$$

$d_i/2$ is the zero point energy

$$d_i = \begin{cases} 1 & \text{for stretches} \\ 2 & \text{for degenerate bends} \end{cases}$$

and $V_{m:n}$ is the resonance coupling term between two modes labeled 1 and 2

$$V_{m:n} = k_{m:n}((a_1^\dagger)^m (a_2)^n + (a_2^\dagger)^n (a_1)^m) \tag{3}$$

Using the Heisenberg correspondence principle,[19,20] the quantum spectroscopic Hamiltonian is transformed to the following semiclassical form

$$H_{m:n} = H_0 + V_{m:n}$$

$$H_0 = \sum_i \omega_i I_i + \sum_i \sum_{j \geq i} \chi_{ij} I_i I_j$$

$$V_{m:n} = 2k_{m:n}\sqrt{(I_1)^m (I_2)^n}\cos(m\phi_1 - n\phi_2) \tag{4}$$

† Part of the special issue "R. Stephen Berry Festschrift".

* To whom correspondence should be addressed. email: kellman@oregon.uoregon.edu.

10.1021/jp0263976 CCC: $22.00 
Published on Web 00/00/0000 PAGE EST: 8.9

The modes not coupled by the resonance can be regarded as "spectator modes" because the number of quanta in these modes is preserved; equivalently, the classical actions associated with these modes are constants of the motion. In the following analysis, we consider only cases with two explicit modes, but the values of the parameters given below in eq 7 can easily be adjusted for the existence of spectator modes.

The existence of a global constant of motion, later referred to as the polyad number, can be demonstrated for the classical Hamiltonian with the help of some simple canonical transformations

$$\sigma\psi = m\phi_1 - n\phi_2$$

$$\sigma\theta = m\phi_1 + n\phi_2$$

$$2I_z = \sigma\left(\frac{I_1}{m} - \frac{I_2}{n}\right)$$

$$2I = \sigma\left(\frac{I_1}{m} + \frac{I_2}{n}\right)$$

$$\sigma = \text{greatest common factor of } m \text{ and } n \tag{5}$$

with $\sigma$ included so that $-\pi \leq \psi \leq \pi$. This results in the transformed Hamiltonian

$$H = C + \alpha I_z + \beta I_z^{\,2} + \delta\sqrt{(I + I_z)^m (I - I_z)^n}\cos(\sigma\psi) \tag{6}$$

with the values of $C$, $\alpha$, $\beta$ and $\delta$ given by

$$C = \left(\frac{m\omega_1 + n\omega_2}{\sigma}\right)I + \left(\frac{m^2\chi_{11} + mn\chi_{12} + n^2\chi_{22}}{\sigma^2}\right)I^2$$

$$\alpha = \frac{m\omega_1 - n\omega_2}{\sigma} + 2\left(\frac{m^2\chi_{11} - n^2\chi_{22}}{\sigma^2}\right)I$$

$$\beta = \frac{m^2\chi_{11} - mn\chi_{12} + n^2\chi_{22}}{\sigma^2}$$

$$\delta = 2k_{m:n}\sqrt{\frac{m^m n^n}{\sigma^{m+n}}} \tag{7}$$

Inspection of eq 6 reveals that there is no dependence of the dynamics on the "fast angle" $\theta$ of eq 5, so the action $I$ is a constant of the motion, and can be treated as a parameter, rather than a dynamical variable. The existence of this additional global action demonstrates the integrability of the system, though we will not solve analytically for the remaining local action (see Joyeux[21] for 1:1, 2:1, and 3:1 resonance local mode actions). The corresponding polyad number is a constant of the motion. The quantum equivalent $P = 2I + 1$ is given by

$$P = \sigma\left(\frac{n_1 + d_1/2}{m} + \frac{n_2 + d_2/2}{n}\right) \tag{8}$$

The quantum Hamiltonian is block diagonal in the polyad number. The number of states within a polyad, i.e., subset of states that have the same polyad number, is given by $[P] + 1$ where $[x]$ is the largest integer $i$ such that $i \leq x$.

## III. Polyad Phase Spheres

With the trivial dependence of the dynamics on the fast angle variable $\theta$ of eq 5, the dynamical arena for a fixed value of the polyad number $P$ is a reduced phase space, the surface of a sphere of radius $I$,[1,4,22,23] with canonical variables $I_z$, $\psi$ of eq 5. By projecting out the conserved polyad number and its conjugate angle, one gets a semiclassical representation on the sphere of each energy level of a polyad. Didactic presentations can be found in refs 24,25. To plot the dynamics on the sphere, it is convenient to change to coordinates $\psi$, $\vartheta$, where $\psi$ is as before and serves as the azimuthal angle, and $\vartheta$ is the longitudinal angle, defined as

$$\cos\vartheta = I_z/I \tag{9}$$

We use $\vartheta$ and $\psi$, which as dynamical variables are noncanonical, only for plotting the phase spheres, but retain the canonical $I_z$, $\psi$ when performing the bifurcation analysis. The spheres shown later will actually be plotted as Mercator projections so that the entire sphere may be viewed at once as phase space "portraits".

The spectrum is represented on the phase sphere as follows. From the quantum Hamiltonian eqs 1−3 the energy levels of the polyad are calculated. Then, using eq 4, for each energy level the solutions for the classical quantities $I_z$ and $\psi$ are solved numerically. Each level is represented on the sphere by a trajectory (or sometimes, multiple trajectories) consisting of the solution sets ($I_z$, $\psi$).

## IV. Classical Dynamical Analysis

In this section, we present the general method used to analyze the dynamical structure of the semiclassical Hamiltonian, including its bifurcation behavior. In the next section, we apply these methods to specific $m$:$n$ resonance cases.

We begin with the notion of the fundamental modes, or natural motions of the system.[26] At low energy, these are the usual anharmonic normal modes. At higher energy, the normal modes abruptly change character, and new anharmonic modes are born in bifurcations. The dynamics of the system is represented on phase spheres, with a distinct sphere for each polyad.[1,5] The structure of the sphere is categorized by its fixed-point behavior; each fundamental mode corresponds to a fixed point in the reduced phase space projected on the sphere. Qualitative changes occur with bifurcations, in which the number and character of the fixed points change. The bifurcations take place with variation of control parameters, to be defined later, appropriate to the spectroscopic Hamiltonian. The complete bifurcation behavior of the Hamiltonian with respect to all possible values of the control parameters constitutes the phase space structure of the Hamiltonian, which is plotted and classified on the catastrophe map. This allows different spectral polyads of the same molecule or several molecules at once to be plotted together and compared visually.[5,6]

**A. Fixed Points and Fundamental Modes.** The phase sphere is a reduced-dimension representation of phase space because it projects out the "fast angle" $\theta$ and the polyad number $P$. Fixed points on the sphere therefore correspond to periodic orbits in the full phase space. For example, at low energy the fixed points correspond to the normal modes. Because of the conserved polyad number, at higher energy, even when there is chaos

(unlike the present situation with just a single resonance and therefore integrable dynamics), it is possible to find analytic expressions for the fixed points[24,27−29] and, therefore, the fundamental modes, including the new modes born in bifurcations of the normal modes. In a chaotic system, organized around the fundamental modes there are an infinite number of subsidiary periodic orbits, which can only be found by numerical integration of Hamilton's equations. Fortunately, these subsidiary orbits can be ignored for many purposes of spectral analysis, because the finite size of Planck's constant means that quantum mechanics "smooths over" the finer details of the classical dynamics.

For the *m*: *n* resonance Hamiltonian (6) the dynamical variables are $\psi$ and $I_z$, and their time derivatives are

$$\dot{\psi} = \alpha + 2\beta I_z + \frac{\delta}{2}(I + I_z)^{m/2-1}(I - I_z)^{n/2-1}[m(I - I_z) - n(I + I_z)]\cos(\sigma\psi) \quad (10)$$

$$\dot{I}_z = \sigma\delta(I + I_z)^{m/2}(I - I_z)^{n/2} \sin(\sigma\psi) \quad (11)$$

Setting them simultaneously equal to zero

$$\dot{\psi} = 0 \quad (12)$$

$$\dot{I}_z = 0 \quad (13)$$

gives the general conditions for fixed points (except at the poles, where we have to be more careful for technical reasons of the coordinates, as discussed shortly). These fixed point conditions will lead to polynomial equations for a finite set of solutions, which we will obtain and characterize according to their location on the phase sphere.

The fixed points are found by solving for the conditions 10−13. To satisfy eqs 11,13 requires

$$\cos(\sigma\psi) = \pm 1, \sin(\sigma\psi) = 0 \quad (14)$$

where the plus sign defines the east hemisphere, the minus sign the west. Combining with (10,12) leads to

$$\alpha + 2\beta I_z \pm \frac{\delta}{2}(I + I_z)^{m/2-1}(I - I_z)^{n/2-1}[m(I - I_z) - n(I + I_z)] = 0 \quad (15)$$

The fixed points lie on great circles, defined by (14), that pass through the poles. The number of great circles is given by $\sigma$, so when $\sigma = 1$ there is a single great circle that intersects the equator at the east and west; when $\sigma = 2$ there are two great circles that quarter the sphere.

It is necessary to be careful in applying the fixed points conditions (12,13) at the poles, because the coordinate system can make things very misleading there. At the poles, $\psi$ can be rapidly changing but, since the poles do not depend on the value of $\psi$, they may still be fixed points. Furthermore, at the north pole

$$I_z = I \quad (16)$$

which from (11) satisfies the fixed point condition (13) that $\dot{I}_z = 0$. At the south pole

$$I_z = -I \quad (17)$$

which again satisfies (13). However, this does not necessarily imply that the action is meaningfully fixed at the pole. An example is seen in the 2:1 resonance system, where the north pole is a fixed point, but the south pole is not.[3−5] The reason is easy to see: a trajectory may pass through a pole with nonzero velocity, meaning the pole is not a fixed point, but $\dot{I}_z$ necessarily will equal zero, simply because one is at the top or bottom of the sphere.

One remedy is to rotate the sphere and apply the conditions (12,13) to the rotated poles; another remedy is to plot phase space profiles, i.e., trajectories on the sphere, and examine the behavior at the poles visually.

**B. Stability Analysis of the Fundamental Modes.** The stability character of the modes associated with the fixed points is important, both to characterize the fundamental modes, and also because a change in stability is the hallmark of a bifurcation, so is a key criterion used in the bifurcation analysis.

The stability of the fixed points is determined in general via the stability matrix.[30,31] Let $f = \dot{\psi}$ and $g = \dot{I}_z$. The stability matrix $M$ is given by the Jacobian

$$M = \begin{bmatrix} f_\psi & f_{I_z} \\ g_\psi & g_{I_z} \end{bmatrix} = \begin{bmatrix} \frac{\partial^2 H}{\partial Iz \partial\psi} & \frac{\partial^2 H}{\partial Iz \partial Iz} \\ \frac{-\partial^2 H}{\partial\psi\partial\psi} & \frac{-\partial^2 H}{\partial\psi\partial Iz} \end{bmatrix} \quad (18)$$

A fixed point is unstable when the eigenvalues are real. Additionally, we have that $g_{I_z} = -f_\psi$ so that the eigenvalues $\lambda_i$ are given by

$$\lambda_i = \lambda_\pm = \pm\sqrt{f_\psi^{\,2} + f_{I_z} g_\psi} \quad (19)$$

The expression for $g_\psi$ is given by

$$g_\psi = \sigma^2\delta(I + I_z)^{m/2}(I - I_z)^{n/2}\cos(\sigma\psi) \quad (20)$$

the expression for $f_\psi$ by

$$f_\psi - = \frac{\sigma}{2}\delta(I + I_z)^{m/2-1}(I - I_z)^{n/2-1}[m(I - I_z) - n(I + I_z)]\sin(\sigma\psi) \quad (21)$$

and the expression for $f_{I_z}$ by

$$f_{I_z} = 2\beta + \delta\cos(\sigma\psi)(I + I_z)^{m/2-2}(I - I_z)^{n/2-2} \times \left[\frac{m}{2}\left(\frac{m}{2} - 1\right)(I - I_z)^2 - 2\left(\frac{m}{2}\right)\left(\frac{n}{2}\right)(I + I_z)(I - I_z) + \frac{n}{2}\left(\frac{n}{2} - 1\right)(I + I_z)^2\right] \quad (22)$$

To evaluate the stability of the fixed points on the great circles, the $I_z$ and $\psi$ obtained from the fixed point conditions (14,15) are inserted in the stability matrix equations (19−22). If a rational torus, i.e., torus filled with resonant periodic orbits, exists at coupling $\delta = 0$, its stability cannot be definitively determined from the equations above because the eigenvalues $\lambda_i$ of the stability matrix are identically zero. An analysis of higher order derivatives or invoking the Poincaré Index Theorem leads to the determination that the rational torus is marginally unstable (Poincaré index = 0) for $I_z \neq \pm I$ and stable for $I_z = \pm I$.

**C. Bifurcations and Catastrophe Map.** Using the preceding formalism we can determine the fixed points and their stabilities for a given polyad, given the parameters $C$, $\alpha$, $\beta$, and $\delta$, which are easily obtained by eq 7 from the fit of the spectroscopic Hamiltonian to data. We want to distill these parameters into the minimum number of control parameters necessary to

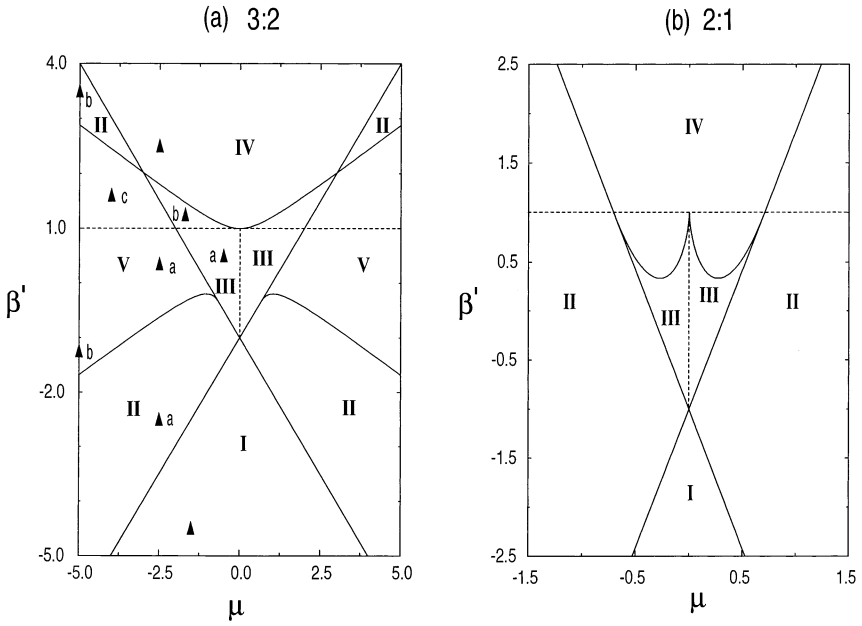


**Figure 1.** (a) 3:2 resonance catastrophe map and (b) the 2:1 resonance catastrophe map. The triangles indicate locations of phase spheres plotted in Figure 2.

characterize the dynamical system. We will then vary the control parameters to see where the fixed points change either their number or stability in bifurcations. The catastrophe map is a plot of where these bifurcations occur as a function of the control parameters.

There are several ways to define the control parameters in a way that minimizes their number, while still being complete. To maintain consistency with earlier papers of Kellman et al., for the 1:1,[4] 2:1[5,3] and 2:2[32,33] resonances, we define the control parameters for the *m*:*n* resonance as follows

$$\beta' = \frac{\alpha}{2\beta I} \tag{23}$$

$$\mu = \frac{\delta}{\beta}(2I)^{(m+n)/2-2} \tag{24}$$

The parameter $\mu$ is referred to as the *coupling* parameter, and is a measure of the resonant coupling between the modes; $\beta'$ is referred to as the *asymmetry* parameter and is a measure of how far the two modes are off-resonance in their zero-order frequencies.[4,5]

The bifurcations of interest to us, either the branching of existing modes or the formation of new modes *de novo* out of phase space (saddle node bifurcation), generally involve the presence of fixed points and a change in stability (however, note the separatrix overlap bifurcation discussed below). The condition for a change in stability is that $\lambda_i = 0$ in the stability matrix analysis. So to construct the catastrophe map, i.e., find the loci of bifurcations as the control parameters are varied, we need simultaneously to satisfy both the zero stability condition ($\lambda_i = 0$) and the fixed point eqs 10,11. The details of this construction and its numerical implementation, though straightforward, are cumbersome, and are placed in the Appendix.

## V. Application to Individual Resonance Hamiltonians

In this section, the preceding formalism is applied to Hamiltonians with various resonance order *m*:*n*. Detailed attention is given to all aspects of the 3:2 resonance, including phase spheres, bifurcations, and catastrophe maps; followed by catastrophe maps for a number of other resonance cases *m*:2 and *m*:4.

**A. Example: The 3:2 Resonance.** The 3:2 resonance is an important resonance between normal modes in the system of two kinetically coupled Morse oscillators,[12−18,34−43] which is a prototype for interesting molecular systems such as the strongly coupled stretch local modes in $CO_2$ or $CS_2$. The 3:2 resonance is strongly implicated (in association with other nearby resonances) with the onset of classical chaos in the coupled Morse system.[15−18] The 3:2 resonance of course can be important in other molecular spectroscopic systems with an accidental 3:2 frequency degeneracy.

The 3:2 resonance catastrophe map is shown in Figure 1(a). For comparison with the 2:1 resonance, Figure 1(b) shows the catastrophe map for the 2:1 Hamiltonian as previously constructed by Kellman et al.[5,3] The first thing to note is that the 3:2 catastrophe map has five zones I−V, whereas the 2:1 map has only four. Second, the two maps are divided by horizontal and vertical dashed lines. We will return to the meaning of these dashed lines shortly.

Despite their differences, the two catastrophe maps are similar. For some of the zones, they share topologically similar phase sphere structure, i.e., structure of stable and unstable fixed points. The zones of the 3:2 map that correspond in this sense to those of the 2:1 map are numbered identically as I−IV in Figure 1. Figure 2 shows representative phase spheres (in Mercator projection) for the 3:2 system. The points on the catastrophe map corresponding to each sphere in Figure 2 are labeled with a triangle in Figure 1. At least one sphere is shown from each zone; cases with multiple spheres from a zone are labeled IIa, IIb, and so forth. Zones I−IV of the two maps have the same structure with regard to their fixed points, as well as the patterns of their quantum spectra.[7] We will abbreviate their discussion, but there are some new twists in the 3:2 system which deserve attention.

For both maps in Figure 1 the vertical dashed line indicates the existence of a rational torus, i.e., a torus filled with resonant periodic orbits, that occurs at zero coupling. The horizontal

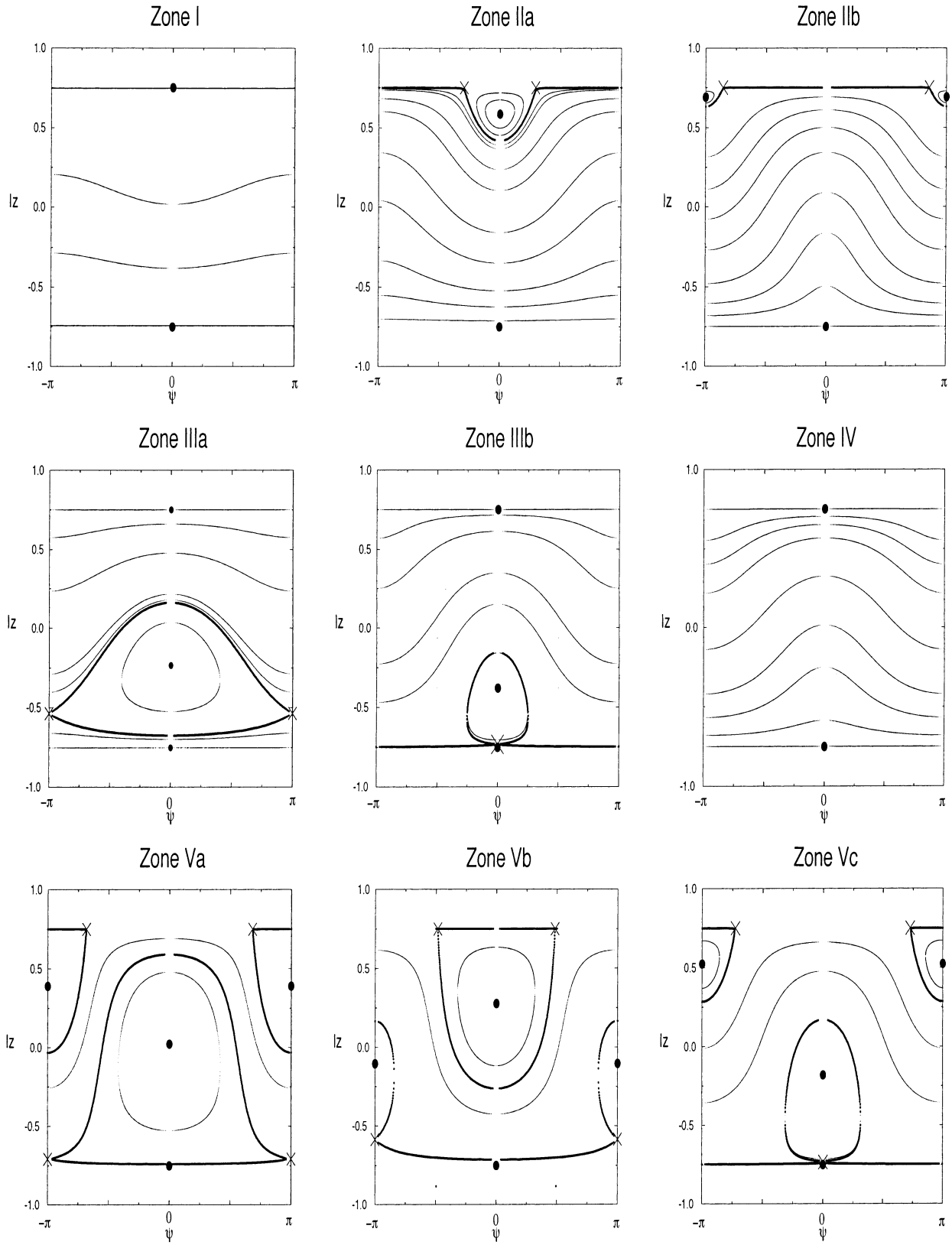


**Figure 2.** Representative phase spheres (as Mercator projections) from different zones of the 3:2 resonance catastrophe map of Figure 1(a). The spheres are labeled by their location on the catastrophe map of Figure 1(a), e.g., sphere IIa is located at triangle "a" in zone II.

dashed line indicates activity involving the south pole. For the 2:1 resonance this is fleeting, occurring when the separatrix passes through the south pole. For the 3:2 resonance, there is more intricate activity at the south pole. Although the number of fixed points remains the same, the east and west fixed points are interchanged, as can be seen in the panels for spheres IIIa,b in Figure 2. The horizontal dashed lines have a connection with behavior seen in spectral patterns that will be discussed below.

*1. Separatrix Overlap Bifurcation and the Augmented Catastrophe Map.* Of particular interest for the 3:2 system is the

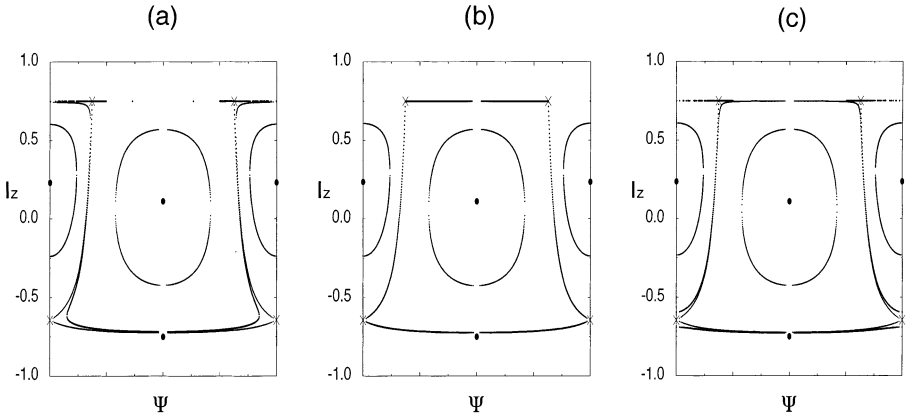


**Figure 3.** Separatrix overlap bifurcation illustrated by a series of phase space portraits that pass through it by a smooth change of control parameters. At the bifurcation, the two separatrices coalesce, eliminating the phase space region between them. The phase space topology is altered after going through this bifurcation although at no time did the existence or stability of any of the fixed points change. For all the plots the coupling parameter, $\mu$, is set equal to $-2.5$, whereas the asymmetry parameter, $\beta'$, is given by (a) $-0.03$, (b) $-0.0237$, and (c) $-0.02$.

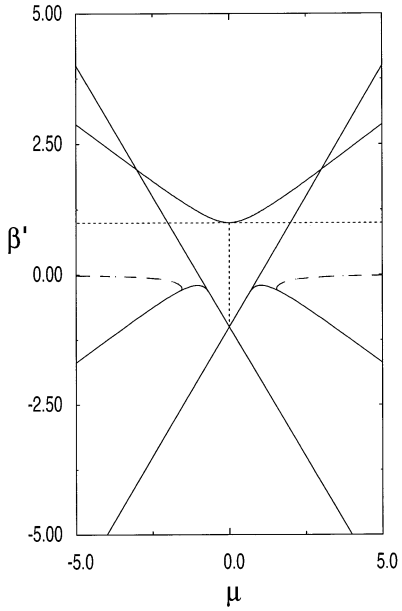


**Figure 4.** 3:2 resonance catastrophe map augmented by the separatrix overlap bifurcation. The map is the same as Figure 1(a) except for the new dashed curves in zone V indicating the locus of the separatrix overlap bifurcation. The phase space plots shown in Figure 3 show the effect of passing through this boundary at $\mu = -2.5$.

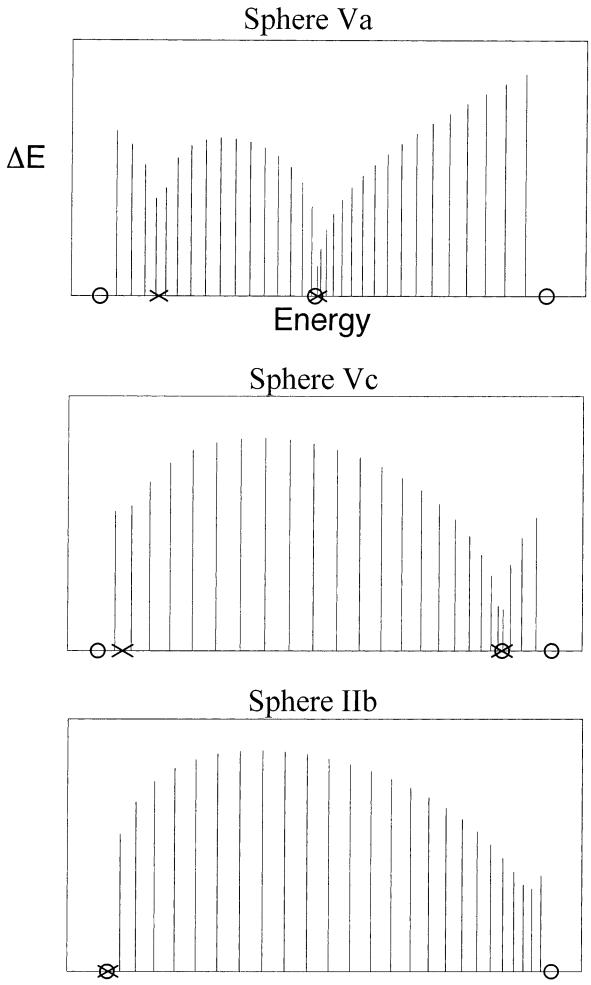


**Figure 5.** Spectral patterns of spacing of adjacent levels for 3:2 catastrophe map zones sampled in Figure 1(a). The spectra are those of individual phase spheres shown in Figure 2. Each "X" represents the energy of an unstable fixed point and associated separatrix on the given sphere; each circle represents the energy of a stable fixed point.

remaining zone V, which exhibits not only new phase sphere structure, but also a novel kind of bifurcation that does not involve a change of stability of the fixed points. Inspection of the phase space plots for spheres from zone Va and Vb in Figure 2 shows that there is some sort of bifurcation taking place. This is a peculiar type of bifurcation because it does not involve a change in the number or stability of the fixed points.

The key is to recognize that this bifurcation involves not the fixed points but rather the other component of the phase space structure, the separatrices—specifically, *overlap* of two separatrices. The phase space portrait at a point where this bifurcation takes place is shown in Figure 3. The bifurcation occurs at the south pole. It is clear that it involves the separatrices, not the fixed points.

To provide a more complete description it is necessary to augment the catastrophe map to take into account this bifurcation involving overlapping separatrices. This separates the catastrophe map into additional regions. The augmented catastrophe map for the 3:2 resonance shown in Figure 4. The added bifurcations due to separatrix overlap are indicated in Figure 4 by the newly added dashed curves in zone V. (Compare with Figure 1(a)).

We should ascertain at this point whether the catastrophe maps constructed by Kellman et al.[5,32,33] for the 1:1, 2:2, and

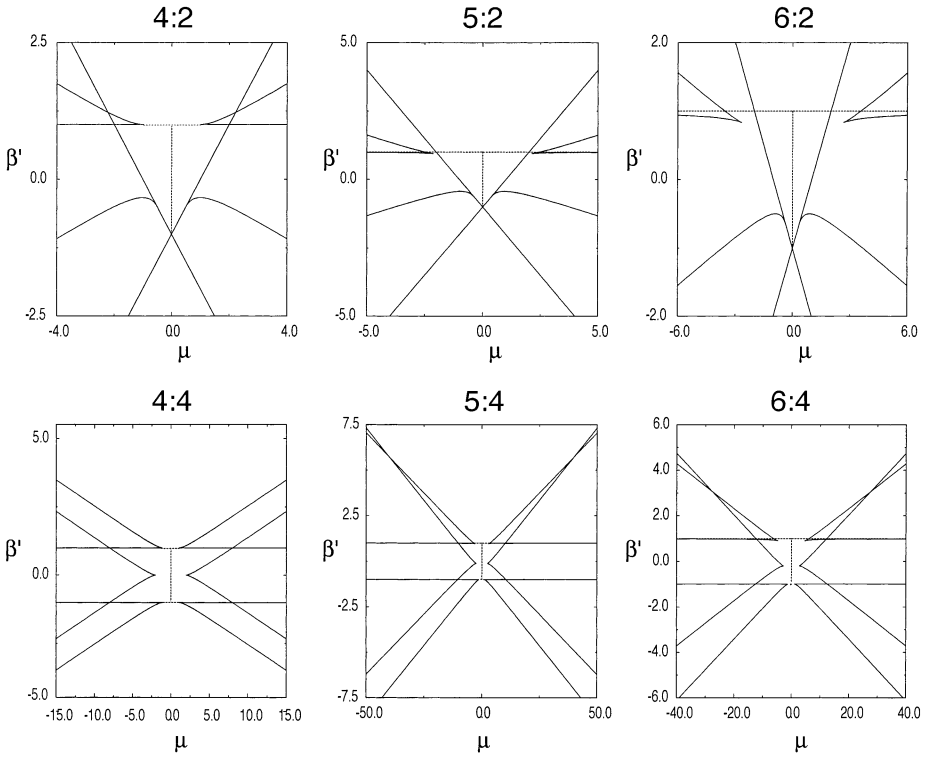


**Figure 6.** Catastrophe maps, analogous to Figure 1(a,b), for the *m*: 2 and *m*: 4 resonances with $m = 4-6$.

2:1 systems also exhibit the separatrix overlap bifurcation. For the 1:1 and 2:1 resonances, there are no catastrophe map zones where there exists more than one separatrix, so these resonances can be eliminated from consideration. The combined 1:1 and 2:2 resonance was examined by Rose and Kellman.[33] The separatrix overlap does occur for this system. This was not noted explicitly in ref 33, but it occurs only where a bifurcation involving fixed points was noted, so no augmentation of the catastrophe map is needed.

*2. Spectral Patterns of the 3:2 Resonance.* The classical phase space structure is reflected in the quantum system. Phase space structure affects spectral patterns, in particular the patterns of energy level differences within a polyad. These patterns were demonstrated previously[7] for the 2:1 Fermi resonance. We now focus on the energy level patterns of the 3:2 resonance, using the previous results on the 2:1 resonance as the starting point. The key point was that the pattern of spacings of adjacent energy levels is indicative of separatrix structure in phase space. A "dip" in the spacing of levels that are "adjacent"—in a suitably defined way having to do with quantum number assignments[7,8]—is the characteristic hallmark of a separatrix.

For the 3:2 system, the spectral patterns in zones I−IV are very similar to those for the 2:1 resonance, reflecting the similar dynamics of corresponding zones in the 2:1 and 3:2 systems.

Zone V of the 3:2 system differs in having two separatrices. This suggests that there should be two minima in the level spacings, and this is indeed the case, as seen in Figure 5, which shows the pattern of adjacent levels for sphere Va of Figure 2.

Another interesting pattern has to do with crossing from a zone with a separatrix, into a zone without a separatrix, but where one sees the remnant of the separatrix in the spectral pattern. In the 2:1 system, in zone IV the energy level pattern has a "pseudo-dip".[7] This is not a true dip, i.e., place where the energy level spacing goes to zero, characteristic of a zero in the classical frequency at a separatrix, and signified by a minimum in the quantum spectrum that goes to zero in the limit $\hbar \rightarrow 0$. Rather, it is characteristic of the *remnant* of a separatrix[7] as catastrophe map zones are crossed. (The pseudo-dip corresponds to an inflection point in an effective potential picture.[7,8] This inflection point is the remnant of a perturbed minimum or maximum in the effective potential and a separatrix on the sphere, as a catastrophe map zone is crossed in a bifurcation which destroys the separatrix.)

The same phenomenon occurs in the 3:2 system. The spectral pattern, Figure 5, of sphere Vc shows a true dip, corresponding to the separatrix at the south pole, Figure 2. The spectral pattern of sphere IIb in Figure 5 looks very similar, but the apparent minimum in the level spacing is a pseudo-dip. It corresponds to the "pinched" character of the phase space near the south pole of the sphere IIb of Figure 2. This pinched phase space is the remnant of the separatrix of sphere Vc.

Zone IV, like zone IIb, has a pseudo-dip in the spectral pattern, the remnant of a separatrix in zone III.

**B. Higher *m*:*n* Resonances.** We now present a host of catastrophe maps for additional *m*: *n* resonance systems, leaving out the detailed description of dynamics in the last two sections. The resonances that we focus on are those that are most important in the dynamics of the normal modes in the system of two kinetically coupled Morse oscillators.[12−18,34−43] Because of the symmetry of the system, *n* is limited to even numbers. These resonances are not limited to the coupled Morse system and may occur in general molecular spectroscopic systems. Generally, we are interested in lower order resonances, as these tend to be stronger and cover a broader range of frequency ratios. The catastrophe maps for the *m*: 2 and *m*: 4 resonance Hamiltonians with $m = 4, 5, 6$ are shown in Figure 6.

The first observation is that the maps for different resonances *m*: *n* tend to be similar for the same value of *n*. The maps for the 3:2 resonance in Figure 1a and the 4:2, 5:2, and 6:2 in Figure 6 all have a similar pattern; the maps for the 4:4, 5:4, and 6:4 in Figure 6 all have a pattern distinct from the *m*: 2 pattern.

There are several observations to be made about the phase sphere structures associated with the catastrophe maps in Figure 6. First, zones at the top and bottom, center, like zones I and IV in Figure 1, have no separatrices. Their phase space structure, while distorted, is that of the zero-order modes. Second, as zone boundaries are crossed toward $\beta' = 0$ (and $|\mu|$ large), additional separatrices may sometimes be added, with the maximal number occurring when $\beta' = 0$. Third, the zone that contains the control parameter origin has at least one hyperbolic fixed point and associated separatrix (for $\sigma \neq 1$ there are at least $\sigma$ (see eq 5) hyperbolic fixed points and $\sigma$ elliptic fixed points forming an island chain). This arises from the breakup into a resonance zone of the zero-order rational torus that exists when $\mu = 0$. Finally, for separatrix overlap to occur in a zone, it is necessary that there exist more than one separatrix for that zone, eliminating zones I−IV as candidates for this type of bifurcation.

The catastrophe maps of Figure 6 can be augmented for the separatrix overlap bifurcation in the same was as done previously in Figure 4 for the 3:2 resonance; the augmented maps for the 4:2 and 5:2 maps are shown in Figure 7.

## Conclusions and Future Work

In this paper, we have analyzed the classical phase space structure of a spectroscopic Hamiltonian for two coupled vibrational modes using bifurcation theory, classified on catastrophe maps, for a variety of higher order resonances not considered in previous work. A type of bifurcation not encountered for lower resonance orders, involving overlap of separatrices rather than change in behavior of fixed points, has been analyzed. Energy level patterns have been associated with the 3:2 resonance, in analogy with the patterns of adjacent level spacings considered earlier for the 2:1 resonance. Catastrophe maps for a variety of resonances (3:2, 4:2, 5:2, 6:2 and 4:4, 5:4, 6:4) have been presented, and relationships and similarities among them discussed.

Energy level patterns associated with phase space structure, including bifurcations, have become useful in understanding and interpreting dynamical information encoded in experimental and computed spectra.[5−9] The catastrophe map is a way of analyzing and presenting the global phase space structure possible for the spectroscopic Hamiltonian of a given resonance. In this way, distinct and sometimes very subtle changes in energy level patterns can be predicted and interpreted; the predictions for the ubiquitous 2:1 Fermi resonance have in fact been observed. It is hoped that the bifurcation and catastrophe map analysis presented here will prove to be similarly useful for higher order resonances.

## Appendix: Bifurcation Analysis And Catastrophe Map for the *m*:*n* Resonance

Conceptually, the algebra involved in performing the bifurcation analysis and representing it on the catastrophe map is relatively straightforward. It involves examination of where the number and stability of the fixed points changes with respect to variation of the control parameters $\mu$, $\beta'$ of (23,24). With the presence of the conserved polyad number, only algebraic equations with analytic expressions need be solved, rather than numerical solution of the equations of motion.[24,27−29] (However, for the general *m*: *n* resonance there are not analytic solutions for the functions involved, so these do need to be solved numerically.)

We begin by rewriting both the fixed point equations (12,-13) and the condition that the stability changes ($\lambda_i = 0$, with $\lambda_i$

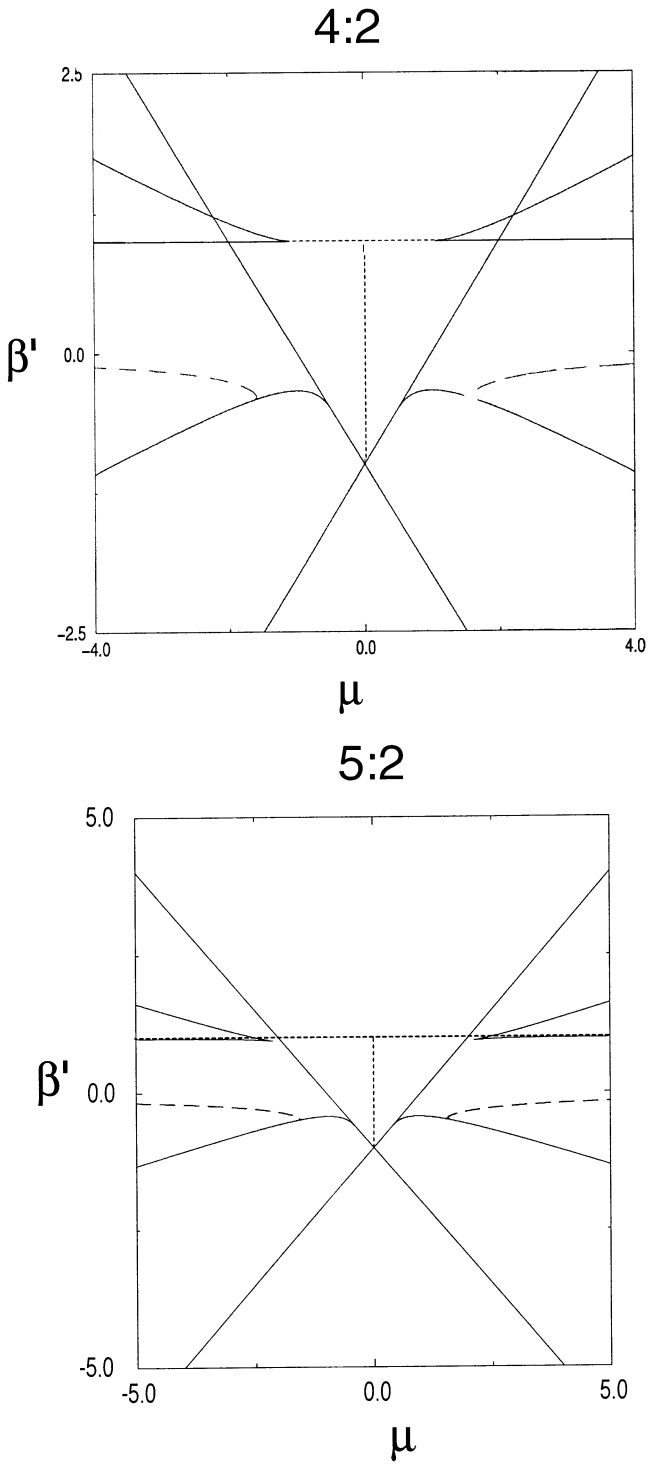


**Figure 7.** Augmented catastrophe maps for the 4:2 and 5:2 resonances. The additional bifurcation due to overlapping separatrices is given by the new dashed curves (compare Figure 6) in the same manner as the augmented 3:2 map in Figure 4.

given by eqs 19−22) in terms of the control parameters $\mu$, $\beta'$ of (23,24) and a parameter that we here call $\gamma$, defined as

$$\gamma \equiv I_z/I \tag{A1}$$

where $|\gamma| \leq 1$ by definition. (The parameter $\gamma$ has the same definition as $\vartheta$ defined earlier in (9) to parametrize the sphere; we employ the two separate symbols $\gamma$, $\vartheta$ to distinguish their

distinct usages.) Writing $\lambda^2$ in terms of these variables (as a precursor to solving for the bifurcation condition $\lambda^2 = 0$), we have

$$\lambda^2 = \frac{\beta^2\mu I^2}{2^{m+n-4}}\left\{\frac{1}{4}\mu(1+\gamma)^{m-2}(1-\gamma)^{n-2}\sin^2(\sigma\psi)[m(1-\gamma) - n(1+\gamma)]^2\sigma^2 + \sigma^2\cos(\sigma\psi)\left[2^{(m+n)/2-1}\sqrt{(1+\gamma)^m(1-\gamma)^n} + \mu\cos(\sigma\psi)(1+\gamma)^{m-2}(1-\gamma)^{n-2}\left\{\left(\frac{m}{2}\right)\left(\frac{m}{2}-1\right)(1-\gamma)^2 - 2\left(\frac{m}{2}\right)\left(\frac{n}{2}\right)(1+\gamma)(1-\gamma) + \left(\frac{n}{2}\right)\left(\frac{n}{2}-1\right)(1+\gamma)^2\right\}\right]\right\} \quad \text{(A2)}$$

Rather than mount a frontal analytic assault on this equation, we next rewrite the fixed point conditions in terms of $\gamma$, $\mu$, and $\beta'$ and use these with (A2) to obtain the bifurcation information we want by means of numerical techniques. We will proceed through the fixed points and their bifurcations in the same order that they were presented in Section IV.

*1. Fixed Points on Great Circles.* The fixed points on great circles are given from (14) by $\cos(\sigma\psi) = \pm 1$, with the additional condition given by eq 15. In terms of $\gamma$, $\mu$, and $\beta'$ this is

$$2\beta I\left\{\beta' + \gamma \pm \frac{\mu}{2^{(m+n)/2}}(1+\gamma)^{m/2-1}(1-\gamma)^{n/2-1}[m(1-\gamma) - n(1+\gamma)]\right\} = 0 \quad \text{(A3)}$$

The bifurcation condition $\lambda^2 = 0$ with (A2) for $\lambda$ becomes

$$2^{(m+n)/2-1}\sqrt{(1+\gamma)^m(1-\gamma)^n} \pm \mu \times (1+\gamma)^{m-2}(1-\gamma)^{n-2}\left[\frac{m}{2}\left(\frac{m}{2}-1\right)(1-\gamma)^2 - 2\left(\frac{m}{2}\right)\left(\frac{n}{2}\right)(1-\gamma^2) + \frac{n}{2}\left(\frac{n}{2}-1\right)(1+\gamma)^2\right] = 0 \quad \text{(A4)}$$

For these equations, we must resort to numerically solving them simultaneously for $\mu$ and $\beta'$. This entails inserting values for $\gamma$ between $-1$ and 1, solving for $\mu$ in (A4), and then inserting both $\gamma$ and $\mu$ into (A3) to solve for $\beta'$. Consideration needs to be given to the vanishing denominators when solving for $\mu$ and $\beta'$, as there are values of $\gamma$ where the catastrophe map curves are discontinuous with respect to parametrization by $\gamma$. These values are easily found via the solution of a quadratic expression in the denominator.

*2. No Coupling.* The condition of no coupling, with $\delta = 0$ in the Hamiltonian (6), implies that $I_z = -\alpha/\beta$ for $|I_z| \leq I$; i.e., $\mu = 0$ and $\gamma = -\beta'$ for $|\gamma| \leq 1$, which finally boils down to

$$\mu = 0; -1 \leq \beta' \leq 1 \quad \text{(A5)}$$

This gives rise to a *rational torus* which undergoes a bifurcation to produce a resonance zone with stable and unstable fixed point when the coupling is nonzero. See ref 31.

**Acknowledgment.** We thank Dr. John Rose for numerous discussions concerning the catastrophe map analysis. We gratefully acknowledge research funding from the Department of Energy Basic Energy Sciences Program.

## References and Notes

(1) Xiao, L.; Kellman, M. E. *J. Chem. Phys.* **1989**, *90*, 6086.
(2) Kellman, M. E.; Xiao, L. *Chem. Phys. Lett.* **1989** *162*, 486.
(3) Kellman, M. E.; Xiao, L. *J. Chem. Phys.* **1990** *93*, 5821.
(4) Li, Z.; Xiao, L.; Kellman, M. E. *J. Chem. Phys.* **1990**, *92*, 2251.
(5) Xiao, L.; Kellman, M. E. *J. Chem. Phys.* **1990**, *93*, 5805.
(6) Child, M. S. *J. Mol. Spectrosc.* **2001**, *210*, 157.
(7) Svitak, J.; Li, Z.; Rose, J. P.; Kellman, M. E. *J. Chem. Phys.* **1995**, *102*, 4340.
(8) Joyeux, M.; Sugny, D.; Tyng, V.; Kellman, M. E.; Ishikawa, H.; Field, R. W. *J. Chem. Phys.* **1999**, *112*, 4162.
(9) Zhou, C.; Xie, D.; Chen, R.; Yan, G.; Guo, H.; Tyng, V.; Kellman, M. E. *Spetrcochimica Acata A* **2002**, *58*, 727.
(10) Rose J. P.; Kellman M. E. Spectral Patterns of Chaotic Acetylene, *J. Phys. Chem. A* **2000** *104*, 10 471.
(11) Kellman M. E.; Rose J. P.; Tyng V. Spectral Patterns and Ultrafast Dynamics in Planar Acetylene *Eur. Phys. J. D* **2001** *14*, 225.
(12) Sage, M. L.; Williams, J. A. *J. Chem. Phys.* **1983** *78*, 1348.
(13) Hedges, R. M., Jr.; Reinhardt, W. P *J. Chem. Phys.* **1983** *78*, 3964.
(14) Hutchinson, J. S.; Sibert, E. L., III; Hynes, J. T. *J. Chem. Phys.* **1984** *81*, 1314.
(15) Matsushita, T.; Narita, A.; Terasaka, T. *Chem. Phys. Lett.* **1983** *95*, 129.
(16) Matsushita, T.; Terasaka, T. *Chem. Phys. Lett.* **1983** *100*, 138.
(17) Matsushita, T.; Terasaka, T. *Chem. Phys. Lett.* **1984** *105*, 511.
(18) Terasaka, T.; Matsushita, T. *Phys. Rev. A* **1985** *32*, 538.
(19) Heisenberg, W. *Z. Phys.* **1925** *33*, 879. Translated In *Sources of Quantum Mechanics*; van der Waerden, B. L., Eds.; Dover: New York, 1967.
(20) Child, M. S. *Semiclassical Mechanics with Molecular Applications*; Oxford University Press: New York, 1991.
(21) Joyeux, M. *Chem. Phys.* **1996** *203* 281.
(22) Jaffe, C. *J. Chem. Phys.* **1988**, *89*, 3395.
(23) Kellman, M. E.; Lynch, E. D. *J. Chem. Phys.* **1988**, *89*, 3396.
(24) Kellman, M. E. Dynamical Analysis of Highly Excited Vibrational Spectra: Progress and Prospects In *Molecular Dynamics and Spectroscopy by Stimulated Emission Pumping*, Dai, H.-L., Field, R. W., Eds.; World Scientific: Singapore, 1995.
(25) Kellman, M. E. "Algebraic Methods in Spectroscopy", *Annu. Rev. Phys. Chem.* **1995**, *46*, 395.
(26) Kellman, M. E. "Internal Molecular Motions" In *Encylcopedia of Chemical Physics and Physical Chemistry*, Moore, J. H., Spenser, N. D., Eds.; IOP Publishing: Institute of Physics, London, 2001.
(27) Lu, Z.-M.; Kellman, M. E. *Chem. Phys. Lett.* **1995**, *247*, *195*.
(28) Lu, Z.-M.; Kellman, M. E. *J. Chem. Phys.* **1997**, *107*, 1.
(29) Keshavamurthy, S.; Ezra, G. S. *J. Chem. Phys.* **107**, *156* 1997.
(30) Tabor, M. *Chaos and Integrability in Nonlinear Dynamics* Wiley: New York, 1989.
(31) Hale, J. K.; Koçak, H. *Dynamics and Bifurcations* Springer-Verlag: New York, 1991.
(32) Li, Z. Ph.D. Thesis, University of Oregon, Eugene, OR, 1991.
(33) Rose, J. P.; Kellman, M. E. *J. Chem. Phys.* **1996**, *105*, 10 743.
(34) Thiele, E.; Wilson, D. J. *J. Chem. Phys.* **1961** *35*, 1256.
(35) Watson, I. A.; Henry, B. R.; Ross, I. G. *Spectrosc. Acta A* **1981** *37A*, 857.
(36) Buch, V.; Gerber, R. B.; Ratner, M. A. *J. Chem. Phys.* **1982**, *76*, 5397.
(37) Buch, V.; Gerber, R. B.; Ratner, M. A. *J. Chem. Phys.* **1982**, *76*, 5405.
(38) Longhi, G.; Abbate, S.; Zagano, C.; Botto, G.; Ricard-Lespade, L. *Theor. Chim. Acta* **1992** *82*, 321.
(39) Abbate, S.; Ghisletti, D.; Giorgilli, A.; Lespade, L.; Longhi, G. *Theor. Chim. Acta* **1993** *87*, 215.
(40) Zembekov, A. A. *Phys. Rev. A* **1990** *42*, 7163.
(41) Zembekov, A. A. *Phys. Rev. A* **1992** *45*, 7036.
(42) Cho, S.-W.; Child, M. S. *Mol. Phys.* **1994** *81*, 447.
(43) Weston, W.; Child, M. S. *Chem. Phys. Lett.* **1996**, *262*, 751.